Stanford Exploration Project, Report 93, November 11, 1997, pages 193–209

Stanford Exploration Project, Report 93, November 11, 1997, pages 193–209

Wave-equation migration: The Kirchhoff approach

Erminia Mallia-Zarb[1]

keywords: *velocity, noise, amplitudes, modeling, algorithm*

ABSTRACT

I developed an algorithm that performs 2-D Kirchhoff migration. For testing purposes I generated synthetic data and tested the algorithm using different migration parameters. Thus my results confirmed that, given the correct parameters, Kirchhoff migration successfully converts the data space back to the image space.

INTRODUCTION

The seismic reflection method of subsurface imaging is made up of three phases: acquisition, processing and interpretation. Acquisition maps the subsurface geology into the common-shot-gather data space. This space bears little visual relationship to the image space, and its S/N is often poor. Routine processing is therefore applied to enhance the data quality and to convert it to a zero-offset data space. Where geological structuring is gentle, this new space shows a close geometrical relationship to the image space and is often the end product of processing. For more complex geology this space represents a geometrically "distorted" image, and further processing is usually needed before a reliable interpretation is attempted. As the relationship between this data space and the image space is defined exactly by the wave-equation, the inverse process becomes possible.

In this report I give a brief mathematical treatment of the Kirchhoff migration algorithm for 2-D seismic data. I illustrate the practical implementation of the process by means of an algorithm that I developed and applied to synthetic seismic data. Furthermore, I show results that I obtained in testing different migration parameters to show the extent of "distortion" and the effect of the modeling-imaging procedure.

[1]**email:** erminia@sep.stanford.edu

THEORETICAL APPROACH

Wave-equation migration techniques consist of two distinct steps:
1. Extrapolation of the wavefield recorded at the surface.
2. Imaging.

The extrapolation process is the solution of the homogeneous scalar wave equation. It calculates the wavefield at any position and time from the knowledge of the wavefield at other positions and times. The imaging process determines the position and time at which the extrapolated wavefield is required.

For a two-dimensional constant velocity medium, the extrapolation formula imaged to time t=0 yields the following equation of migration,

$$P_{out}(x_0, z_0, 0) = \left[\left(\frac{\partial}{\partial t} \right)^{\frac{1}{2}} \frac{1}{(2\pi)^{\frac{1}{2}}} \int \frac{cos\theta}{r^{\frac{1}{2}}} P_{in} \left(x - x_0, 0, t - \frac{r}{v} \right) dx \right], \tag{1}$$

where x_0 and z_0 are the spatial location and depth of the image point. $P_{in}(x-x_0, 0, t-r/v)$ is the unmigrated wavefield measured at the earth's surface, $P_{out}(x_0, z_0, 0)$ is the migrated wavefield, $cos\theta$ is the obliquity factor,$cos\theta = z_0/r$, and $r^2 = (x - x_0)^2 + {z_0}^2$.

Thus the Kirchhoff method implied by the above equation reflects a summation over a surface. It contains the half-derivative $(\partial/\partial t)^{\frac{1}{2}}$. This operator is equivalent to a filter with a constant $\pi/4$ phase delay and an amplitude spectrum proportional to the square root of frequency. The migration equation shows that the effect of migration in the (x,t) domain is an amplitude-weighted summation combined with a frequency filtering that incorporates a constant phase shift. The amplitude weighting decays as $1/r^{\frac{1}{2}}$, as shown by the integrand of equation (1).

PRACTICAL IMPLEMENTATION

In practice, 2-D Kirchhoff migration is carried out by summing the amplitudes in (x,t) space along the diffraction curve that corresponds to Huygen's secondary source at each point in (x,z) space. For zero-offset sections, the moveout at a source-receiver point a distance x from the apex of a diffraction hyperbola at time t_0 is given by:

$$t^2 = {t_0}^2 + \frac{4x^2}{v^2}, \tag{2}$$

while for common-offset sections, the moveout is given by:

$$t = \left[\frac{(x + s/2)^2}{v^2} + \frac{{t_0}^2}{4} \right]^{1/2} + \left[\frac{(x - s/2)^2}{v^2} + \frac{{t_0}^2}{4} \right]^{1/2}, \tag{3}$$

where s is the value of offset and v is the velocity at the apex of the hyperbola.

Before summation, each sample is scaled by the obliquity factor, $cos\theta$, and the spherical spreading factor $(1/vt)^{1/2}$. After summation the output section is convolved with a filter whose amplitude-frequency response is proportional to the square root of frequency, with a constant phase delay of $\pi/4$. The latter corresponds to the half-derivative that was mentioned earlier on.

Some practical considerations

The following is a brief discussion of the parameters that need to be taken into consideration in order to optimize the results of migration.

1. Migration aperture width

Theoretically, a diffraction hyperbola extends to infinite time and distance. However in practice only a truncated hyperbolic summation path is considered. The choice of aperture is usually made by considering the maximum dipping events and the size of diffractions present on the input data.

2. Velocity errors

The use of a low migration velocity results in an incomplete collapse of diffractions, and dipping events are only partially repositioned to their true location. Converseley, if the velocity used is too high, diffraction hyperbolas are overmigrated and on sections these are manifested as inverted hyperbolas, or “smiles”. High velocity also results in excessive lateral shifts of dipping events, and higher dips than the actual dips of the subsurface reflectors.

3. Spatial aliasing

Spatial aliasing on migration of field data is minimized by the right choice of CMP trace interval. Another way of minimizing the aliasing effect is by doing trace interpolation before migration.

4. Ambient noise

Considering the summation of random noise along a hyperbolic curve, the final summation is independent of the curvature of the summation trajectory, since random noise amplitude is uniform over the region of the hyperbola. Therefore after migration the noise background is actually reduced by the spherical spreading factor. In a medium where velocity increases with increasing time, the velocity factor in the amplitude scaling factor results in a greater reduction of noise towards the bottom of the section, where the velocities are higher. However background noise becomes more coherent in regions of high velocities. At high velocities the summation hyperbola is very nearly flat. Summation along the curve emphasizes the lower wave numbers, so that the data appears smeared and lateral resolution becomes limited. Therefore noise coherency due to migration is more severe in the bottom section. Another possible adverse effect on a migrated section is shown as “smiles”. These are due to sparsely distributed bursts of amplitude in the input section.

5. Length of profile

If the section to be migrated is too short, this will result in insufficient space for dipping events to move during migration. Another adverse effect is that the effective aperture near the boundaries of the section will be smaller than the aperture width used to migrate the rest of the data. The smearing effect due to this condition contaminates a large percentage of the final migrated section, since the latter is too short. Migration algorithms assume that the data outside the side boundaries of the input stacked section is of zero amplitude or zero gradient. If traces of zero amplitude are appended to the edges of the section, dipping events can move freely into the zero-amplitude region during migration.

KIRCHHOFF MIGRATION OF SYNTHETIC SEISMIC DATA

Several two-dimensional seismic sections were modeled and migrated using the Kirchhoff summation method. Migration was carried out on two types of record sections, zero-offset and common-offset gathers. Finally tests were carried out to show the effect of migration parameters on the output migrated section.

Generation of synthetic seismic data

A modeling technique was developed to generate the seismic response of some simple geological structures. Each model reflector was considered as being made up of a continuum of Huygens' secondary sources. At each point on the reflector a diffraction hyperbola was generated with a moveout determined by the velocity function defined at that point. The aperture was taken as the whole section. Each point on the hyperbola was weighted by the factors described in the Kirchhoff Integral formula, namely the obliquity factor and the directivity factor. The superposition of the generated hyperbolas produced the seismic response of the specified structure.

All seismic records presented in this study are made up of one hundred traces having a total length of 2 s. The trace interval is 25 m, and the time sampling interval is 4 ms. The vertical axis represents two-way travel time. The reflection wavelet was designed as a Ricker wavelet with a peak frequency of 18 Hz. The reflection coefficient of each model was taken as unity.

Migration algorithm

An algorithm was developed to migrate the synthetic data sections. The algorithm was adapted to handle temporal and spatial variations in velocity. The migration of model record sections was carried out using parameters defined in the modeling process, so that the process was the exact inverse of that used to generate the unmigrated sections. The migration aperture was taken across the whole seismic section.

Constant velocity sections

Figure 1 shows a simple flat horizon as a reflection profile on a depth section converted to two-way traveltime. Figures 2 and 3 show, respectively, the zero-offset and common-offset seismic response of the reflector. In generating the seismic response in Figure 3, the common offset distance was taken as 1000 m. The reflector is assumed to lie in a medium of constant velocity equal to 2000 m/s.

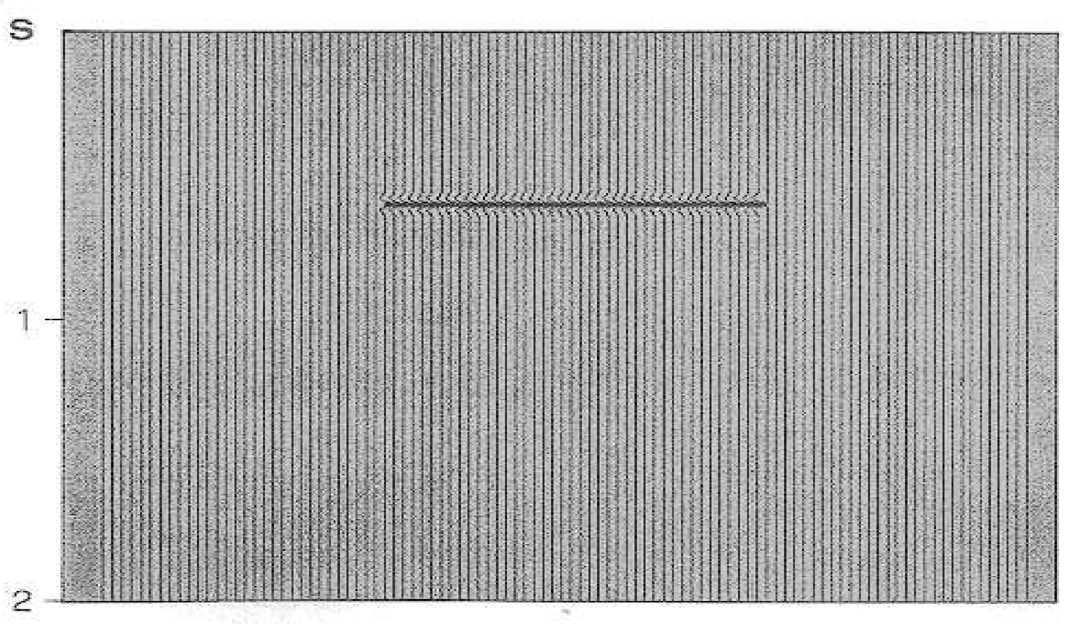

Figure 1: Horizontal reflector (constant velocity, 2000 m/s). erminia-f3-8a [NR]

The zero-offset response shows that the reflected horizon remains unshifted in time. However the edges give rise to diffracted energy, and the ends of the reflector are now not so clearly defined. Figure 4 shows that migration successfully collapses the diffractions, and the edges of the horizon are once more shown to lie at their true lateral positions.

Referring to the common-offset seismic response in Figure 3 and comparing this section to the zero-offset response in Figure 2, the whole reflector is shifted down the section by a time interval which is determined by the source-receiver separation. It is also evident that seismic diffractions in nonzero-offset records behave in a similar way to those shown on zero-offset sections. Figure 5 shows the output migrated image. All points on the reflector have been correctly repositioned in time and space. Diffracted energy has been completely removed, and the lateral termination points of the horizon have been redefined accurately.

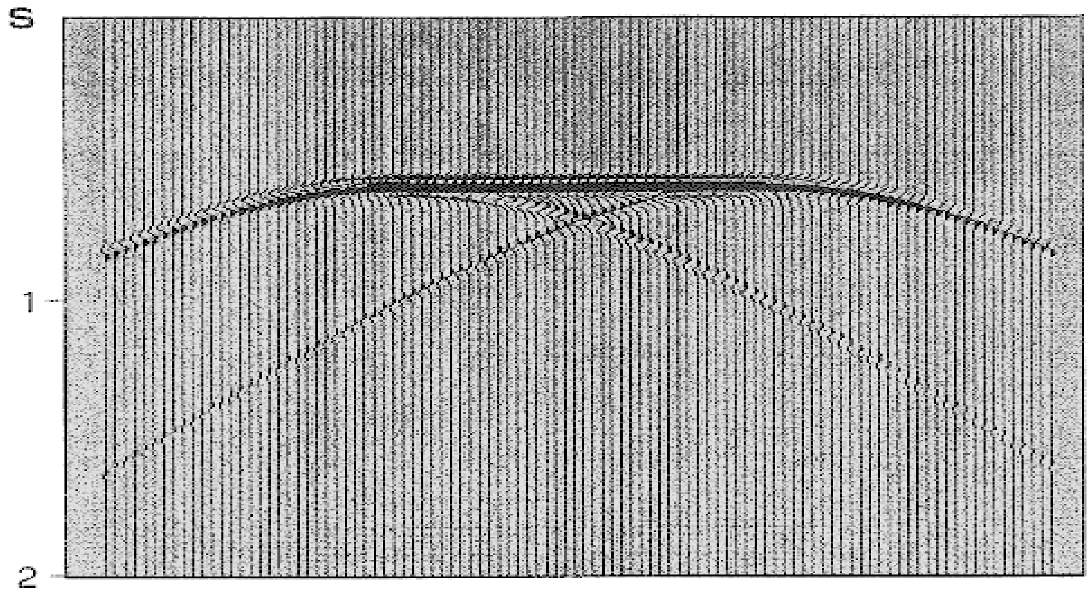

Figure 2: Zero-offset seismic response of horizontal reflector model. erminia-f3-8b [NR]

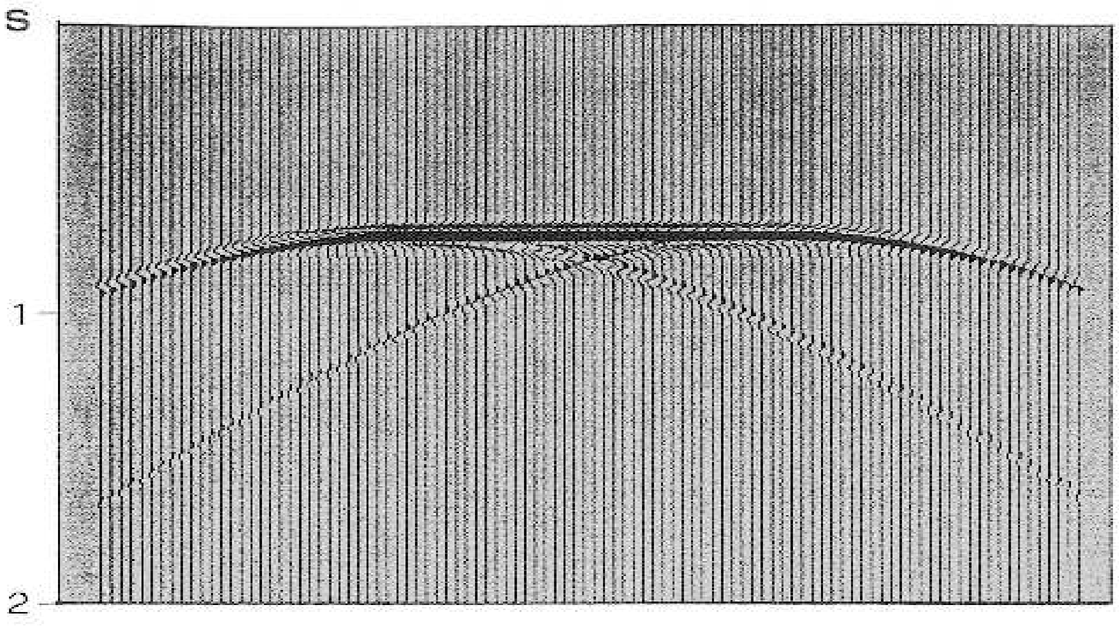

Figure 3: Common-offset seismic response of the horizontal reflector model. erminia-f3-18a [NR]

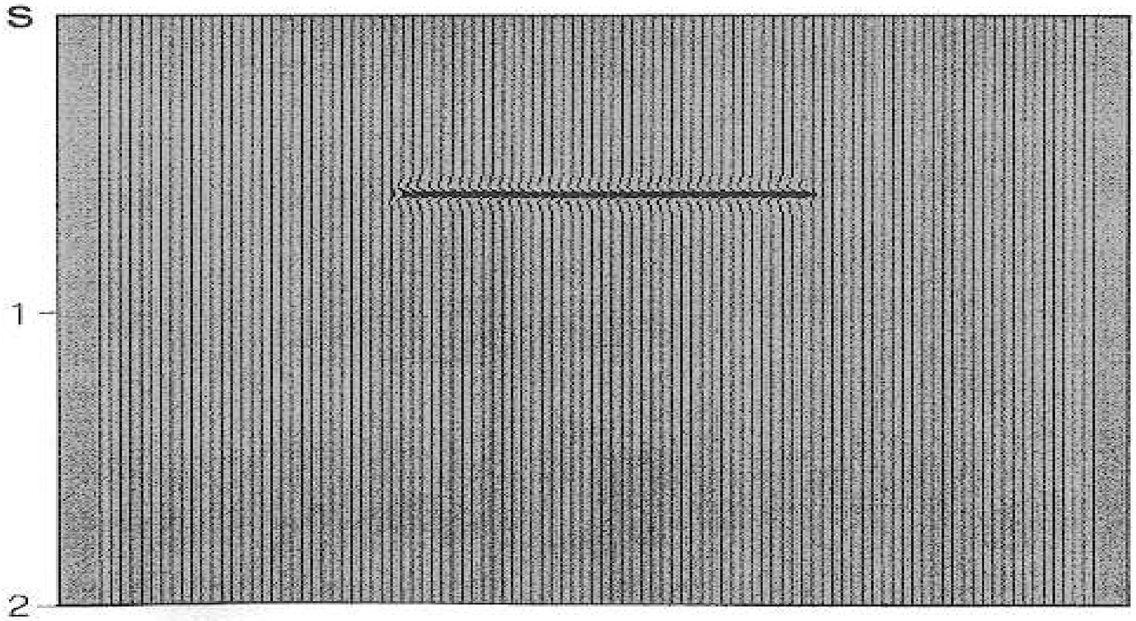

Figure 4: Migration of zero-offset section. erminia-f3-8c [NR]

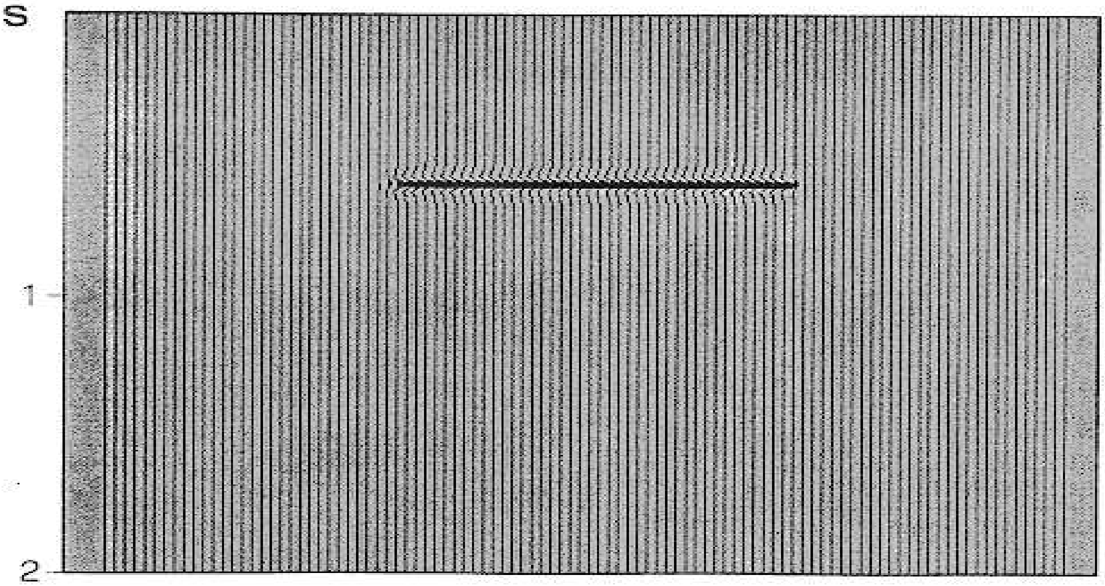

Figure 5: Migration of common-offset section. erminia-f3-18b [NR]

Variable velocity sections

The migration algorithm was adapted to handle variations in migration velocity (which is equivalent to rms velocity) with observed travel times and spatial locations. This was done by defining the velocity as a function of observation time and space, respectively. Illustrations for both cases shall be made on the same dipping reflector model shown in Figure 6.

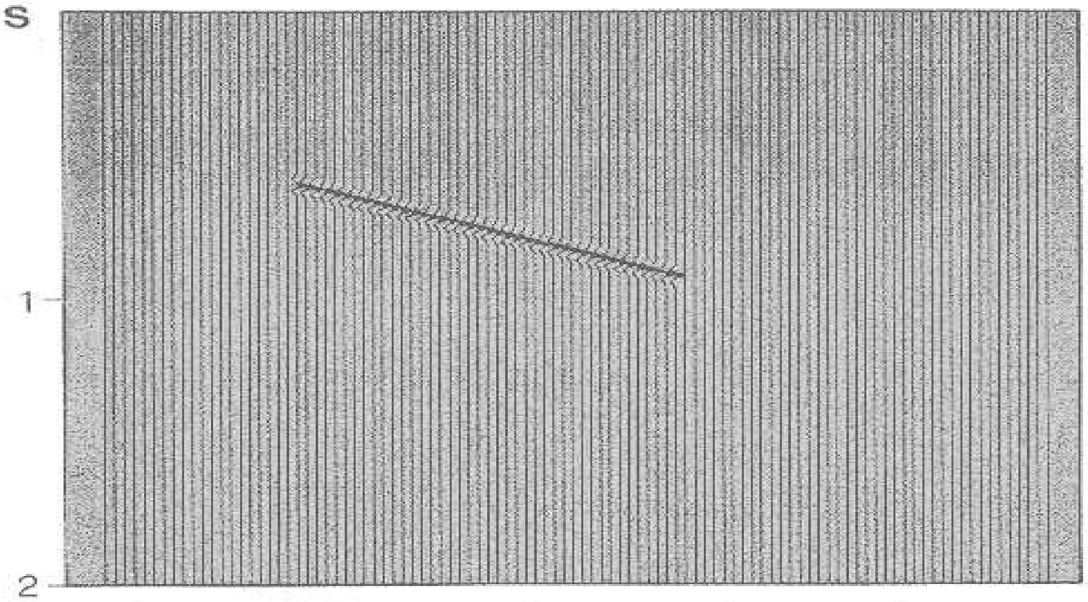

Figure 6: Dipping reflector (dip, 8 ms/trace). erminia-f3-11a [NR]

Figure 7 shows the zero-offset seismic response of this model. The velocity function used was taken from a real seismic data record section, and it varies only with observation time. The same velocity function was used to migrate this section, and the output record is shown in Figure 8. The dipping reflector is correctly repositioned, temporally and spatially, to its true subsurface location.

The same results were obtained when spatial variations in velocity were taken into account. The migrated output section (Figure 10) of the zero-offset section shown in Figure 9 is the correct image of the model dipping reflector.

Thus it has been shown that if the velocity function is known accurately both in observation time and spatial location, Kirchhoff migration is performed successfully on stacked data. Similar results can be shown for the case of non-zero offset data.

Testing for Kirchhoff migration parameters

After having successfully imaged the sections shown above using the correct migration parameters, tests were carried out to show the effect of variations in migration

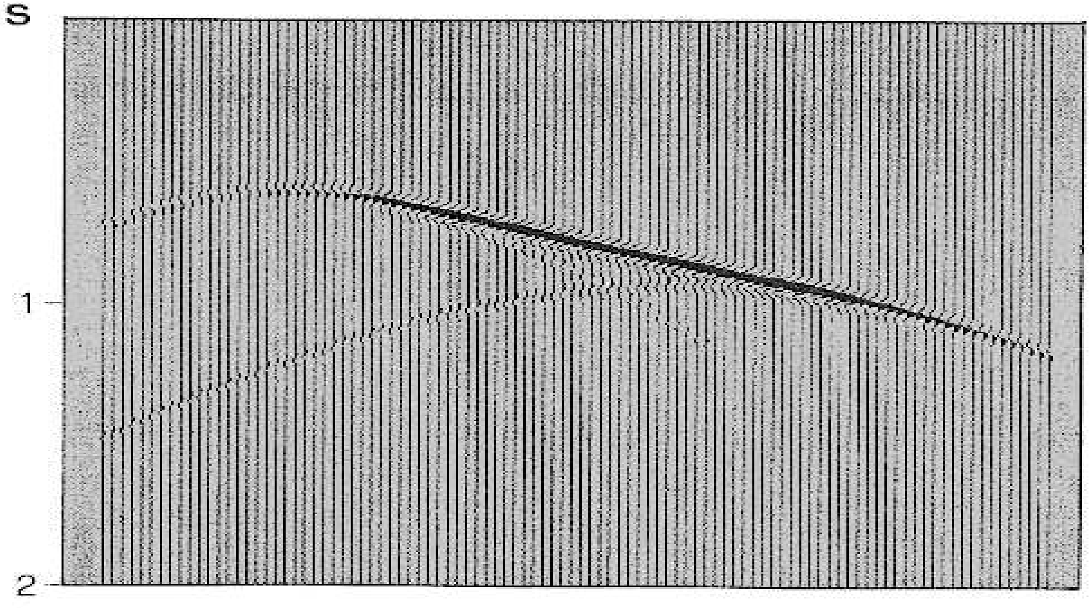

Figure 7: Zero-offset seismic response of dipping reflector model (velocity function, time-variant). erminia-f3-15a [NR]

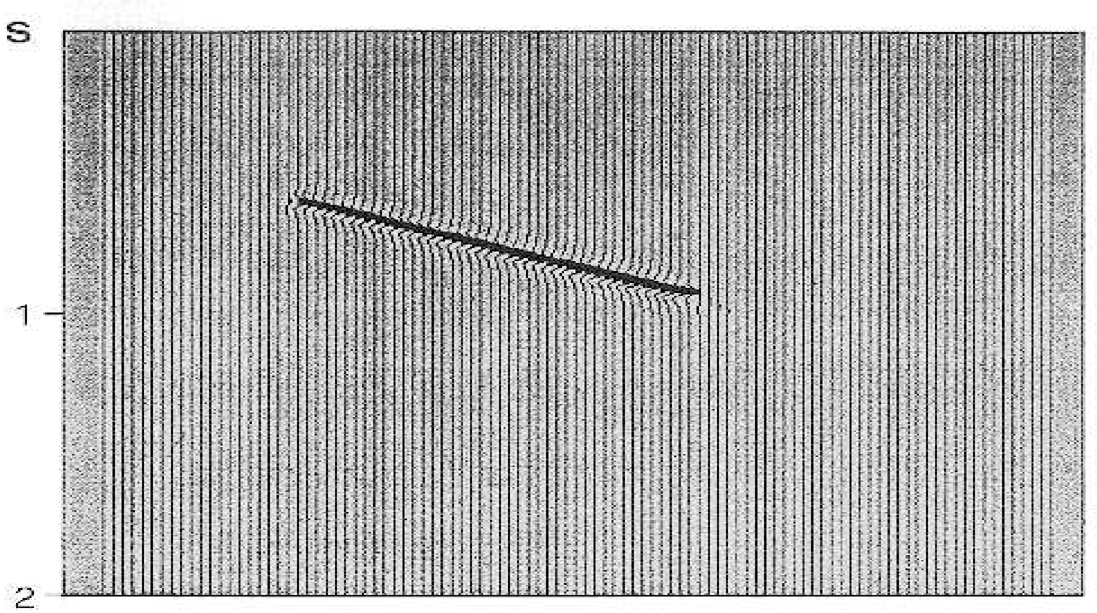

Figure 8: Output migrated section of Figure 7. erminia-f3-15b [NR]

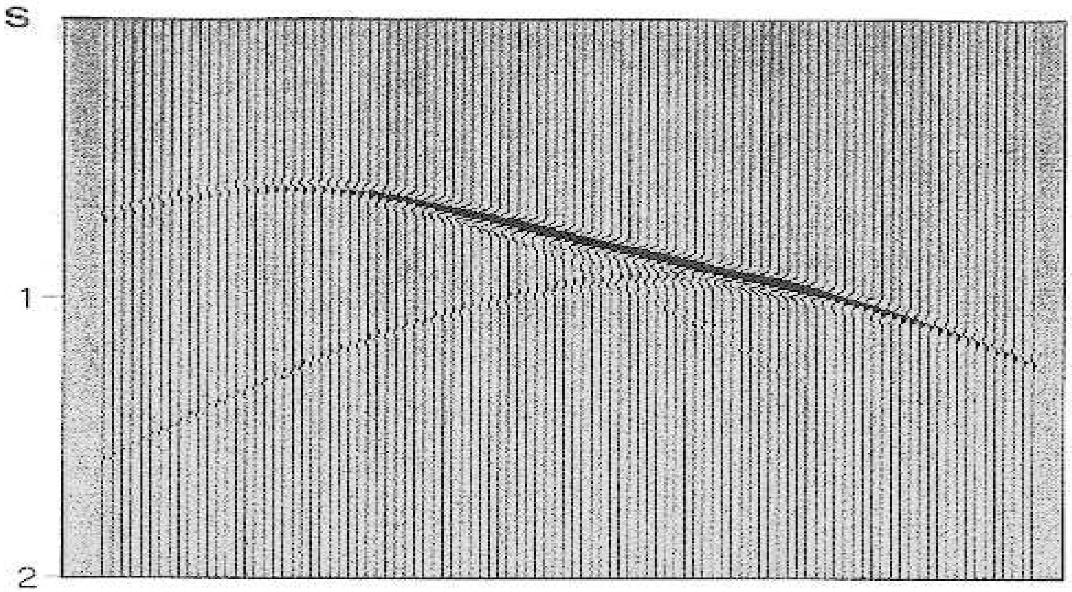

Figure 9: Zero-offset seismic response of dipping reflector model (velocity function, space-variant). erminia-f3-16a [NR]

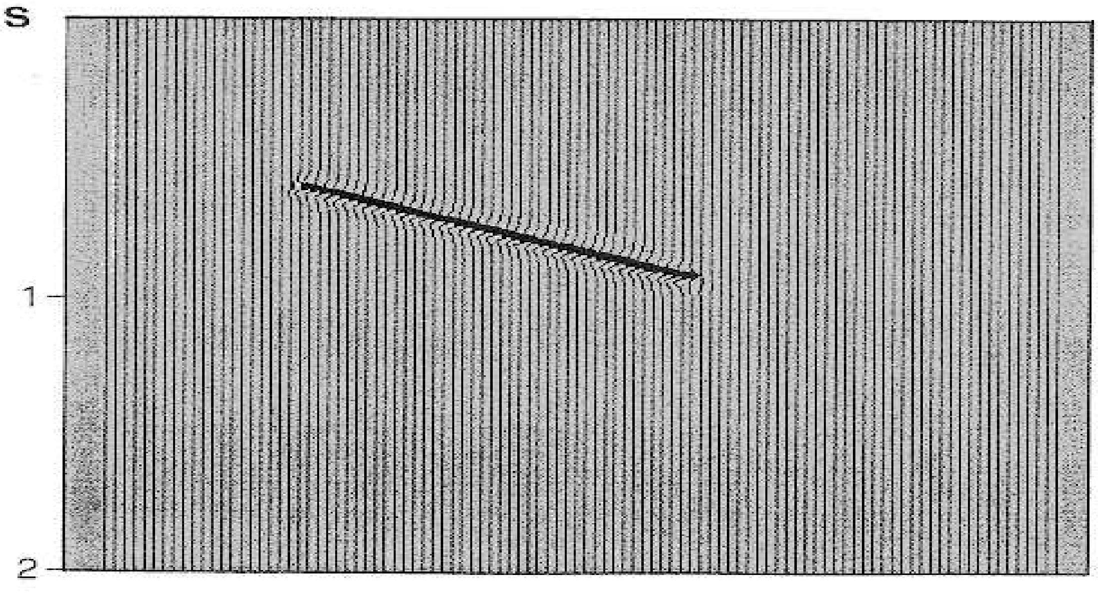

Figure 10: Output migrated section of Figure 9. erminia-f3-16b [NR]

parameters on the output migrated section. The migration algorithm was tested for the choice of aperture width and migration velocity, and for the effect of migration on background noise present in the input data section.

Aperture width

The zero-offset response of the dipping reflector, shown in Figure 7, was migrated with a half-aperture width of 25 and 5 traces respectively as shown in Figure 11 and Figure 12. The choice of a small aperture results in undermigration. As the migration aperture becomes smaller, the edge diffractions become more pronounced. Also, the reflector is not fully shortened to its actual length, and the dip remains smaller than the true structural dip. As the aperture increases, the reflector is migrated closer to its true location and the output section is improved.

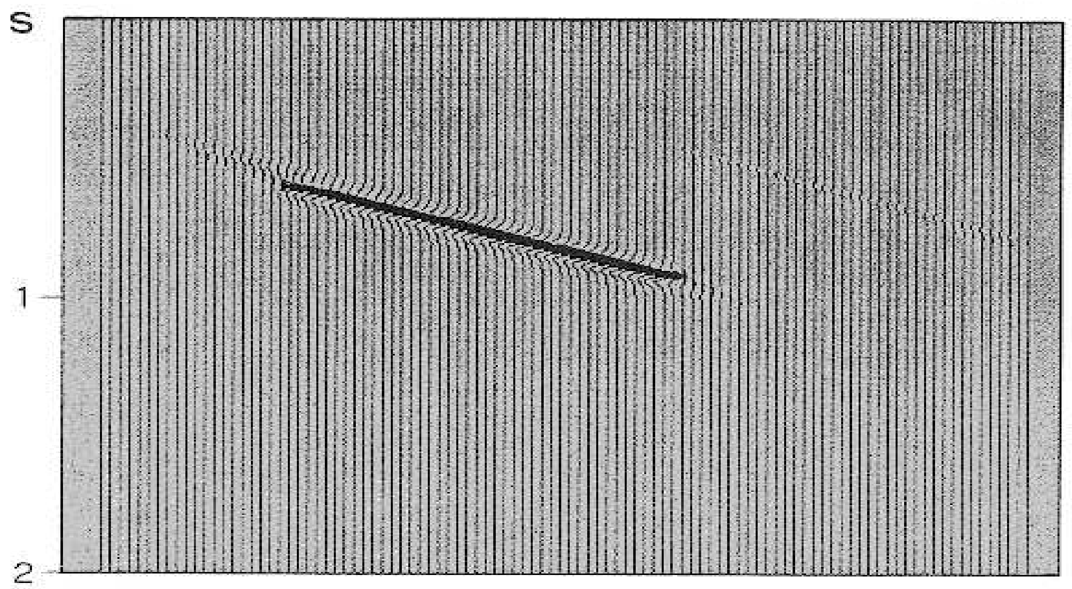

Figure 11: Migration of the zero-offset response of the dipping reflector shown in Figure 7 using a limited migration aperture width (half-aperture, 25 traces). erminia-f3-23a [NR]

Velocity function

The migration algorithm was tested for the effect of distortion with the use of an incorrectly low or high migration velocity. For this purpose, testing was carried out on the zero-offset response of the dipping reflector shown in Figure 6, for a medium of constant velocity equal to 2000 m/s.

Figure 13 shows the result of migration using a velocity that is 20 percent lower than the true velocity. The reflector is only partly shifted updip and remains less steep

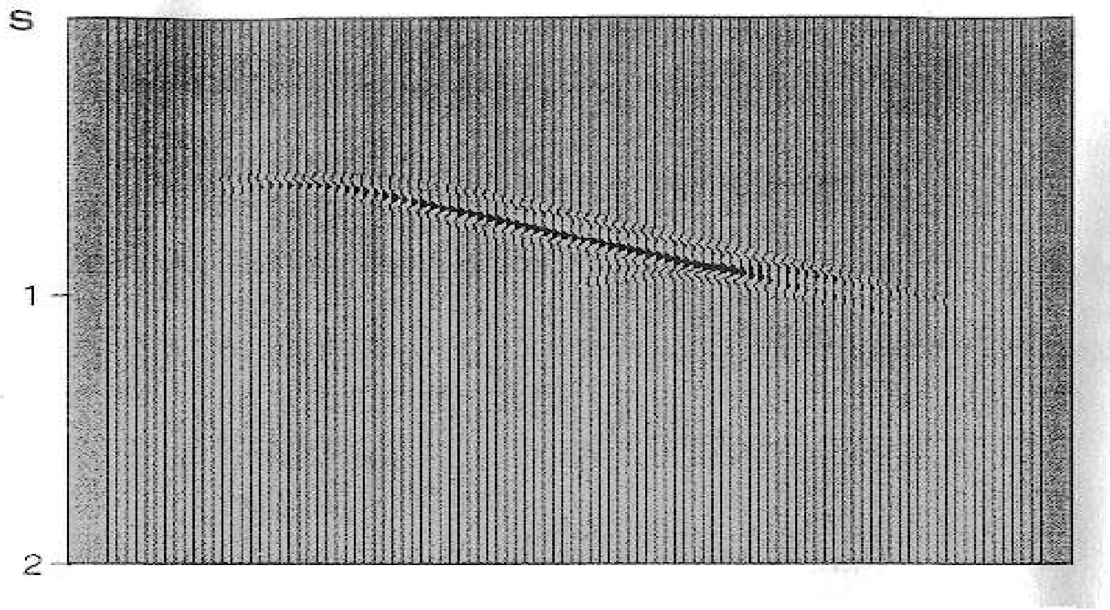

Figure 12: Output migrated section (half-aperture, 5 traces). erminia-f3-23b [NR]

than the true inclination of the model. Besides, diffraction events are still present at the edges.

Figure 14 shows the opposite effect on using a 20 percent higher migration velocity. Now the dipping reflector is overmigrated. It has in fact moved further updip than its true location, and the edges of the reflector are smeared. The edge effects now show up as “smiles”.

Ambient noise

Random noise was added to the zero-offset section of the horizontal reflector in Figure 2, where the medium was assumed to have a constant velocity equal to 2000 m/s. The noisy section is shown in Figure 15. The corresponding migrated section in Figure 16 shows that the noise in the section has decreased in amplitude as a result of migration. Note that a constant scaling factor was applied to the section so that the noise could actually be seen, hence the very large amplitudes of the reflector. It can be seen from the figure that noise amplitudes become lower down the section. This time-variant reduction of noise is due to the time factor in the spherical spreading term of Kirchhoff summation, as was explained earlier on.

The zero-offset seismic response of the same reflector was generated using a time-variant velocity function, where velocity increases with increasing traveltime. Its output migrated section is shown in Figure 17. Here the variable velocity factor results in a greater reduction of noise towards the bottom of the section, where the velocities

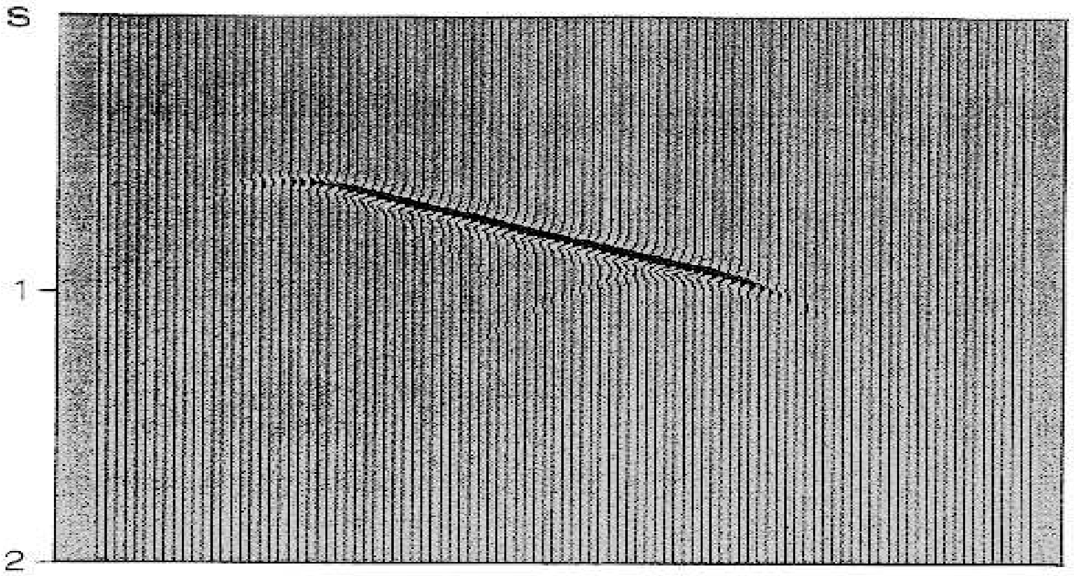

Figure 13: Undermigration of dipping reflector in Figure 6 (migration velocity, 20 percent lower than true medium velocity). erminia-fvel1 [NR]

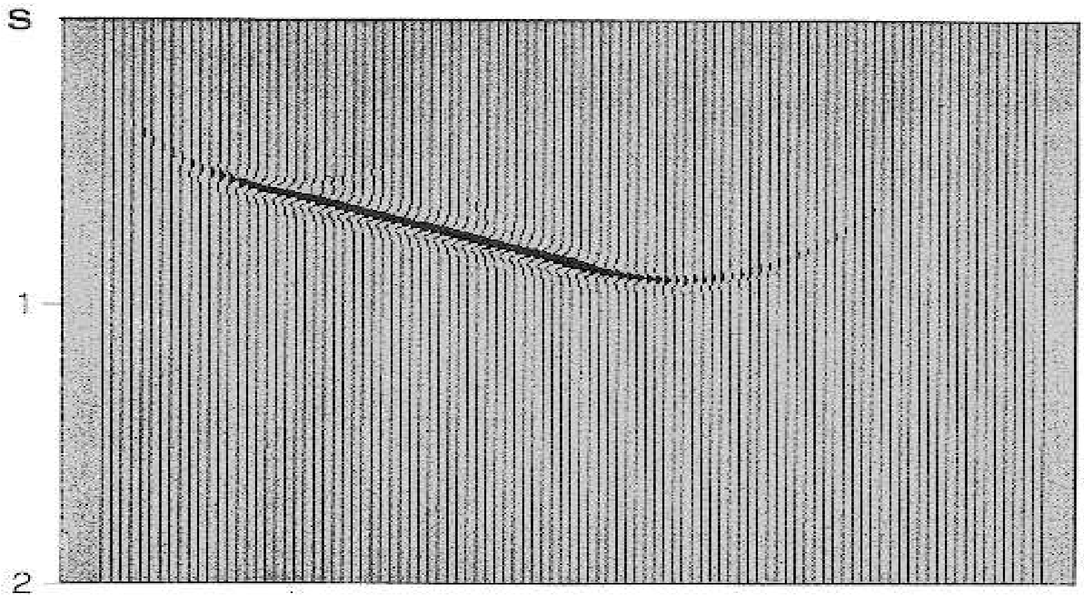

Figure 14: Overmigration of dipping reflector (migration velocity, 20 percent higher than the true medium velocity). erminia-fvel2 [NR]

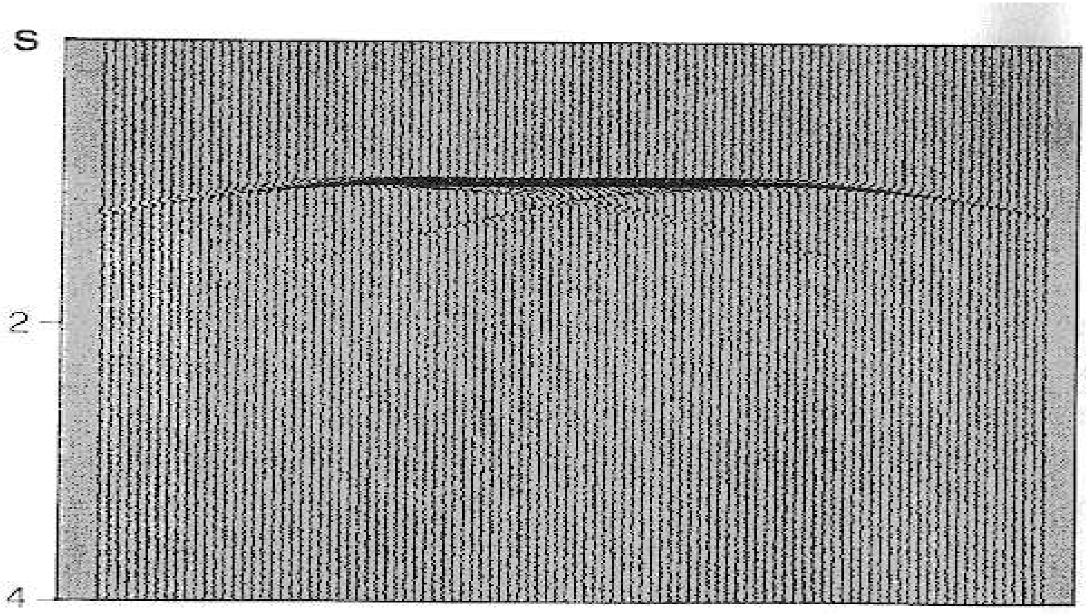

Figure 15: Zero-offset seismic response of a horizontal reflector (shown in Figure 2) with random noise added to the section. erminia-f3-26a [NR]

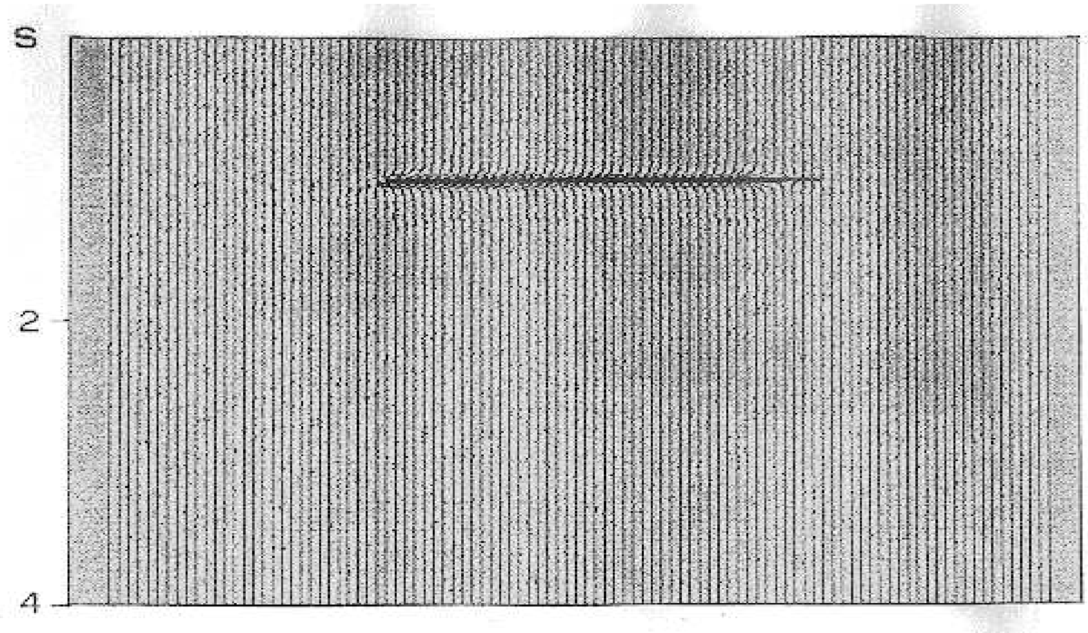

Figure 16: Migration (constant velocity medium). erminia-f3-26b [NR]

are higher. However the background noise looks more coherent as its amplitude is decreased, that is, in the deeper parts of the section.

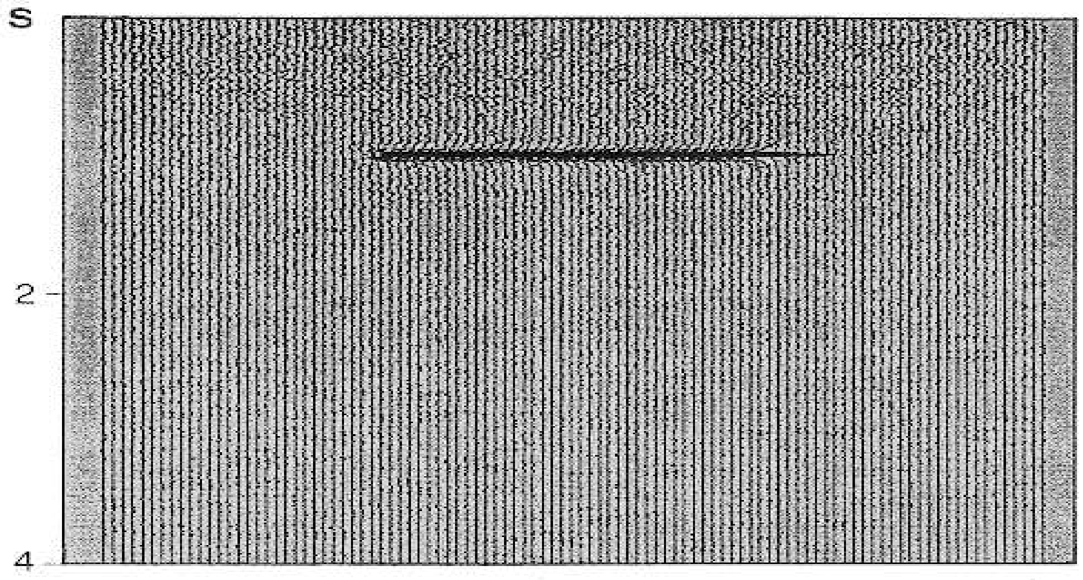

Figure 17: Migration (medium velocity increases with increasing time). erminia-f3-26c [NR]

CONCLUSIONS

In view of the results that I have shown, I conclude that with the use of the right migration parameters, the application of Kirchhoff migration to 2-D synthetic seismic data results in an exact inversion of the data space to the image space, as predicted by theory. Furthermore, the incorrect use of migration parameters leads to undesirable artifacts in the output image, and above all to the incorrect imaging of the input data.

This work was done for my undergraduate thesis, and now I am investigating the application of Kirchhoff migration to 3-D seismic data.

ACKNOWLEDGMENTS

I would like to thank Dr. Godwin Debono of the University of Malta for his advice and guidance throughout this project.

REFERENCES

Berryhill, J.R., 1976, Diffraction response for nonzero separation of source and receiver: Geophysics, **42**, 1158-1176.

Dobrin, M.B. and Savit, C.H., 1988, Introduction to geophysical prospecting: McGraw-Hill Book Company.

Hatton, L., Worthington, M.H. and Makin, J., 1986, Seismic data processing theory and practice: Blackwell Scientific Publications.

Hilterman, F.J., 1970, Three-dimensional seismic modeling: Geophysics, **35**, 1020-1037.

Jakubowicz, H. and Levin, S., 1982, A simple exact method of 3-D migration - theory: Geophysical Prospecting, **31**, 34-56.

Kanasewich, E.R., 1975, Time sequence analysis: The University of Alberta Press.

Ricker, N., 1940, The form and nature of seismic waves and the structure of seismograms: Geophysics, **5** , 348-366.

Schneider, W.A., 1977, Integral formulation for migration in two and three dimensions: Geophysics, **5**, 348-366.

Trorey, A.W., 1970, A simple theory for seismic diffractions: Geophysics, **35**, 762-784.

Vetterling, W.T., Teukolsky, S.A., Press, W.H. and Flannery, B.P., 1989, Numerical recipes: the art of scientific computing: Cambridge University Press.

Yilmaz, O., 1993, Seismic data processing: Society of Exploration Geophysicists.